AIAA Aviation
16-20 June 2014, Atlanta, GA
44th AIAA Fluid Dynamics Conference

Numerical Investigation of Unsteady Heat Transfer on a Double Wedge Geometry in Hypervelocity Flows

Jeffrey R. Komives*, Ioannis Nompelis†, and Graham V. Candler‡
Department of Aerospace Engineering and Mechanics
University of Minnesota, Minneapolis, MN, 55455

In recent experiments performed at the University of Illinois, nitrogen and air flows over a double wedge geometry at Mach numbers varying from 4-7 and stagnation enthalpies varying from 2.1-8.0 MJ/kg were investigated. Selected cases from these experiments are simulated using US3D to ascertain the ability of state-of-the-art finite-volume hypersonic flow solvers to replicate experimental results. Two-dimensional simulations predict an unsteady separation and shock-shock interaction under both reacting and non-reacting conditions. The numerical solutions reach a time-periodic solution for certain experimental conditions. Good agreement is observed between experiment and two-dimensional simulations of the Mach 7 flow conditions when the simulations are limited to the experimental run-time. When run to a large number of flowtimes, the agreement is poor. Three-dimensional simulations of these free-stream conditions show non-uniformities in the wedge boundary layer during flow development.

I. Introduction

Recent experiments by Swantek and Austin[1] performed at the University of Illinois hypersonic facility investigated heat transfer and flowfield structure of hypervelocity flows of air and nitrogen over a 30-55° double wedge. Measurements were made and Schlieren images were obtained for flows in a variety of free-stream enthalpies and free-stream Reynolds number conditions. The overall aim of their work was to create a dataset suitable for validating numerical simulations of high-speed flows. In the course of their experiments, Swantek and Austin identified that many of their experiments exhibited unsteadiness or large run-to-run variability. Recently, simulations by Badr and Knight[2] using the commercial package GASPex showed good agreement for two-dimensional simulations of the nominally Mach 7, 2.1 MJ/kg total enthalpy (M7_2) free-stream condition assuming perfect gas flow. Agreement was poorer when simulating the nominally Mach 7, 8 MJ/kg total enthalpy (M7_8) free-stream condition. Additionally, Patil, et al.[3] investigated these same two test conditions using a Direct-Simulation Monte Carlo (DSMC) particle approach. Their work showed good agreement in shock structure and wall heating at the M7_8 free-stream condition when the simulation was terminated at 100 μsec, however continuing the simulation showed unsteadiness in the flowfield that would not have settled during the experimental runtime. Furthermore DSMC simulations at the lower enthalpy M7_2 condition showed a dynamic flowfield throughout the simulation. The aim of the present work is to examine the ability of state-of-the-art numerical simulations[4] to replicate the results of these experiments.

The flow over a double wedge at hypersonic conditions has been studied extensively in the past.[5–7] An oblique shock originates from the tip of the geometry and a detached bow shock is formed because of the presence of the second wedge. The two shocks interact to form a compression shock that impinges on the geometry. The adverse pressure gradient that is seen by the flow along the first wedge causes the flow to

*Graduate Student, AIAA Member
†Research Associate, AIAA Senior Member
‡Professor, AIAA Fellow

The views expressed in this article are those of the author and do not reflect the official policy or position of the United States Air Force, Department of Defense, or the U.S. Government.
DISTRIBUTION STATEMENT A. Approved for public release; distribution is unlimited

separate, creating a separation-bubble at the corner. Under certain conditions, the flow is known to become unsteady as seen previously in experiments on double-cone geometries.[8] Under the present experimental conditions, the separation that forms continuously grows and leads to an unsteady flowfield. The process that leads to the unsteady separation quickly becomes chaotic, in part because of the presence of a separation shock that is formed when the supersonic flow behind the oblique shock interacts with the separation zone. This shock affects the separation and leads to a highly non-linear feedback mechanism that continuously alters the flowfield. Under these conditions, the flow does not stabilize to a steady-state; this effect is seen both in experiment and in our simulations.

In the present work, we use the implicit finite-volume hypersonic flow solver US3D to compute the flow-fields at the given experimental conditions. Carefully constructed grids were tested for grid-convergence, keeping in mind that the flow-fields are indeed unsteady. As a result, our discretization involves a grid that is stretched near the wall to resolve the boundary layer and has uniform and isotropic spacing in the interior where shock-shock interactions and the shear-layer are present. We use a single grid that adequately resolves the boundary layer by ensuring that the y^+ remains order one for the entire flowfield and for all time simulated.

II. Numerical and Physical Modeling

We study hypersonic flows with nonequilibrium and high enthalpy (or "real-gas") effects using computational fluid dynamics (CFD). A mass conservation equation is solved for each of the species that are possible products of the chemical reactions under these conditions, namely N_2, N, O_2, O, and NO. We solve the mass conservation equations along with the momentum and energy equations. Dalton's law is assumed as the equation of state for a mixture of perfect gases. Rotational energy is in equilibrium with the translational modes at the mixture temperature T. We solve a separate equation for vibrational energy of the mixture where the vibrational energy for all species is in equilibrium at a common temperature T_v. The Landau-Teller[9] model for V-T relaxation is used with Millikan-White[10] inter-species relaxation rates. The chemical reactions involving dissociation and recombination take a modified Arrhenius form and the Park rates are used as well as the Park $T - T_v$ coupling model.[11] Viscosity coefficients are calculated from Blottner's fits[12] using Wilke's semi-emperical mixing rule.

The equations are discretized with a finite volume method. The inviscid fluxes in US3D can be evaluated using one of several methods. These are: a second order accurate modified Steger-Warming[13] method, a second order accurate central kinetic energy consistent method,[14] or a fourth- and sixth-order accurate gradient reconstruction methods. The equations are integrated to steady state with a second-order implicit time-stepping using the DPLR method.[15] For the present work, the baseline results use inviscid fluxes which are computed using a modified second-order Steger-Warming formulation. Time is advanced using a second-order implicit Euler time integration with point relaxation.

II.A. Free-stream Conditions

In this work, the M7_2 and M7_8 free-stream conditions were examined. The post-shock tunnel conditions were determined by Swantek and Austin[16] using the facility characterization by Dufrene et al.[17] Information pertaining to these conditions is presented in Table 1. In this table, a flowtime is defined as the ratio of the face length (.0508 m) to the free-stream velocity, and the Reynolds number is based on the wedge face length.

II.B. Grid Construction

In the experiments by Swantek and Austin,[1] variability and unsteadiness was observed at certain free-stream conditions. Anticipating that the flowfield may be unsteady, the grid used in this study was designed to have isotropic spacing away from the double wedge. The baseline two-dimensional grid was created with 512 nodes in the streamwise direction and 256 nodes in the wall-normal direction. The nodes are clustered near the wall to ensure proper viscous spacing and are equally spaced away from the wall, outside of the boundary layer. The wedge was modeled as an isothermal no-slip wall at 300K with a symmetry line leading to the stagnation point. Details of the grid are shown in figure 1.

To examine the effect of grid resolution, a refined grid was created with 768 nodes in the streamwise direction, and 386 nodes in the wall-normal direction. The placement of the first node off of the wall was

Table 1. Selected free-stream conditions adapted from Swantek and Austin[1]

	M7_2	M7_8
Mach number	7.11	7.14
Stagnation enthalpy, MJ/kg	2.1	8.0
Static temperature, K	191	710
Static pressure, kPa	0.391	0.78
Velocity, m/s	1972	3812
Density, kg/m^3	0.0071	0.0038
Reynolds number (Re$_L$)	55,880	22,098
Test time, μsec (flowtimes)	327 (12)	242 (18)

held fixed, and is the same as the baseline grid.

To study the three-dimensionality of the flowfield, a three-dimensional grid was generated with 512 nodes in the streamwise direction, 256 nodes in the wall-normal direction, and 256 nodes along the model in the spanwise direction, with clustering to increase the density of points near the sides of the double wedge. The sides of the double wedge were modeled as slip walls. The width of the double wedge was set to match that of the actual test article, which had a 2:1 aspect ratio based on its face length. The two buffer blocks on either side of the wedge span thirty nodes with matched node spacing next to the wedge. The 3-D grid is represented in figure 2. A summary of all grid dimensions is presented in table 2.

Table 2. Summary of two- and three-dimensional grid extents used in simulations

	Baseline	Refined	3D
Wall-normal	255	385	255
Streamwise	511	767	511
Spanwise	N/A	N/A	255
Total Cell-count	133,305	295,295	45.8M

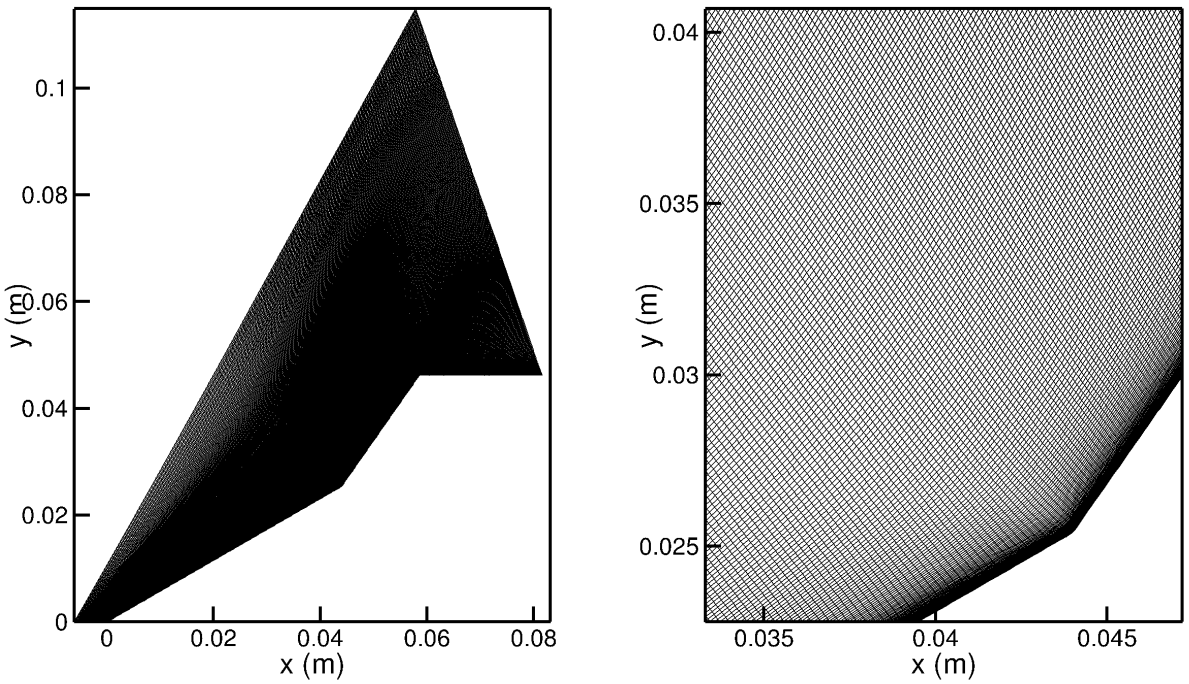

(a) Complete grid extents

(b) Detail showing mesh spacing near wedge intersection

Figure 1. Baseline two-dimensional double wedge grid of 512×256 points. Full grid (a) and enlargement at the juncture showing stretching at the wall that transitions to isotropic spacing in the interior (b).

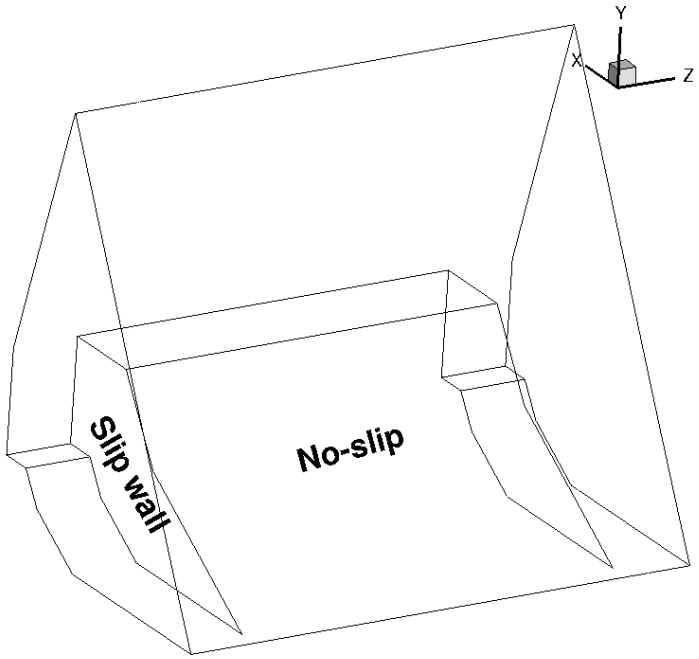

Figure 2. Three-dimensional grid showing wall boundary conditions used in the simulations

III. Solutions Run to Approximate Flowtimes

Solutions were run to approximately the same length of time as the duration of the experiment. The solutions were obtained by a second-order point implicit time-integrator with a CFL number of 100, and are therefore not considered to be time-accurate. At this CFL number, the physical timestep was 12 *nsec* for all simulations.

The experimental data used for comparison in this section were obtained by time-averaging thermocouple signals after the tunnel start-up process.[16] The results of the simulation, however, are presented at an instant in time with no averaging applied. We indicate the instant at which simulation data is shown for each case. Note that in the simulations, time is measured from the beginning of each run, which has an impulsive start with uniform free-stream conditions everywhere. Thus, time does not coincide with any temporal reference in the experiments.

It is very difficult to precisely mimic the actual start-up process of the experimental facility. The expansion tunnel starts by shock-heating a gas that rests in the acceleration section of the tube, which then flows past the model prior to the arrival of the actual test gas.[11] Although it is possible in principle to simulate the entire start-up process of the expansion tunnel, including the flow through the nozzle,[18] we assume that the start-up process does not affect the flowfield during the actual test-time. In the present work, the simulations were started impulsively where the computational domain was initialized to match the inlet conditions.

III.A. Mach 7, 2 MJ/kg Enthalpy

For the M7_2 free-stream condition, the test gas is modeled as a perfect gas, not allowing any dissociation or energy storage in vibrational energy. Swantek and Austin[1] report up to 327 μsec of test time at this condition, with the final Schlieren image being captured at 270 μsec.[16]

Figure 3 compares the measured and predicted heating at $t = 270$ μsec for both nitrogen and air. The experimental value is averaged at each station once the flow has started over the double wedge, while the simulated values represent instantaneous data. The data from Swantek and Austin are plotted with 8% error bars, which is the stated accuracy of their heat-flux measurements.

First examining the nitrogen case, heat transfer predicted on the forward part of the wedge matches that measured in the experiment. Our simulation slightly overpredicts heating at the fourth thermocouple location. The remaining measurements on the forward face of the double wedge show a much larger spread than the measurements further upstream. This coincides with the simulated region where wall heating irregularities indicate vortical structures within the separation region. On the aft face of the double wedge experimental measurements show a heating peak with a maximum value of 1.3 MW/m^2. This peak corresponds to the location and shape of the simulated heating peak. In the simulation, the shape of the heating profile on the aft wedge modulates over time such that the averaged heating levels at any given station on this face are higher than represented in this instantaneous representation.

Examining the air case we see that the simulation predicts wall heating indicative of separation just prior to the second thermocouple location, which closely matches the experiment. For the remainder of the separated region, predicted wall heating closely matches that measured in the experiment. On the aft face of the double wedge the predicted shape and amplitude of the heating profile also very closely match that measured in the experiment.

Figure 4 compares the computed shock structure with the experimentally captured Schlieren images for the nitrogen case. The simulated results show separation and the associated separation shock at approximately the same location shown in the Schlieren images. Note that the angle of the separation shock is different in the simulation and the experiment. Also, slight curvature of the separation shock is visible in the Schlieren image, which is an indication of possible unsteadiness in the experiment. The simulation predicts multiple vortical structures within the separation region resulting in the formation of several shocks and a very unsteady flowfield in the separation region. Weak oblique shocks are also visible inside the separation zone in the experimental Schlieren image; the visible shocks are originating at approximately the locations of thermocouples C and D. The simulated bow shock has a much larger stand-off distance from the aft face of the wedge than was seen in the experiment. Swantek[16] notes that in this experiment, the location of the oblique shock, separation shock and bow shock all varied with time. However, the streamwise location of the triple-point did not move significantly in the streamwise direction.

Figure 5 compares computed and measured shock structures using air as the test gas. The simulated post-shock flowfield is very similar to that predicted using nitrogen as the test gas for this condition. The

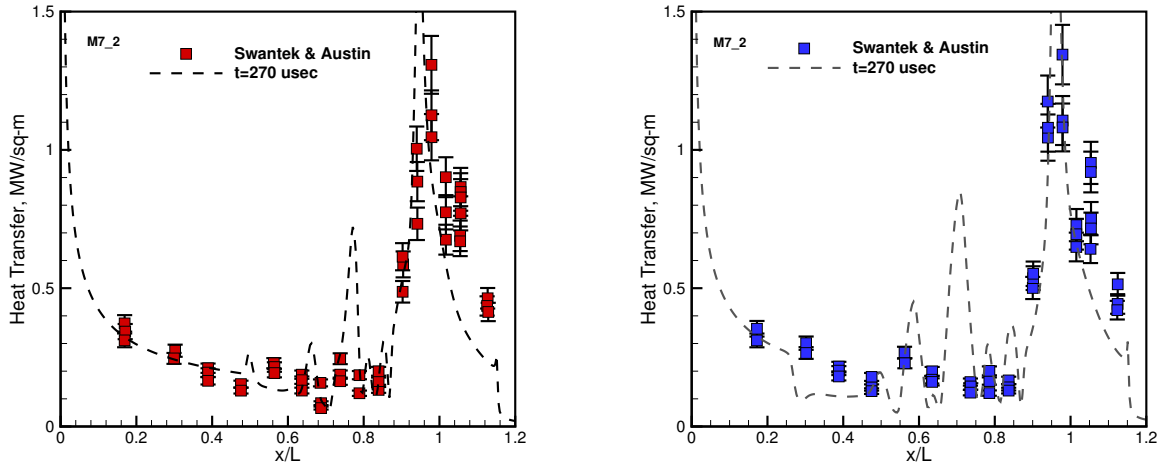

(a) Nitrogen (b) Air

Figure 3. Comparison of instantaneous predicted wall heating with measured values for the M7_2 free-stream condition at 270 μsec. Simulations with nitrogen (a) and air (b) as the test gas are shown.

fact that both simulated flowfields show the same flow structure is consistent with experimental observations by Swantek.[16]

III.B. Mach 7, 8 MJ/kg Enthalpy

For the M7_8 free-stream condition, the test gas is modeled as a "real" gas, including effects of vibrational excitation, dissociation and recombination. Swantek and Austin[1] report up to 242 μsec of test time at this condition, with the final Schlieren image being captured at 200 μsec.[16]

Figure 6 compares the measured and predicted heating at $t = 200$ μsec for nitrogen and $t = 160$ μsec for air. The experimental value is averaged at each station once the flow has started over the double wedge, while the simulated values represent one instant in time. The data from Swantek and Austin are plotted with 8% error bars, which is the stated accuracy of their heat-flux measurements.

Examining the simulation in nitrogen, heating is slightly underpredicted on the forward face of the wedge upstream of separation. Simulated heating values indicate that separation has occurred approximately at the third thermocouple location. The predicted wall heating within the separation region matches the level of the experimental measurements, with the exception of the fourth and fifth thermocouples. Also, the predicted heating exhibits variation within the separation zone that is not seen in the experiments. Simulated heating on the aft face of the wedge has the same peak amplitude and location as was seen in the experiment. The width of the peak heating profile is not the same in the simulation as was seen experimentally, however. Similarly to the M7_2 simulations, the heating profile on the aft face of the wedge modulated throughout the entire simulation run, sweeping the heating peak over the region of experimentally measured peak heating.

For the air case, the simulation at 160 μsec showed the best agreement with the experimental measurements. Heating is underpredicted on the first two thermocouples on the forward face of the wedge. The predicted heating on the remainder of the front face matches very well with experiment. The experiment shows elevated heating on the fifth thermocouple indicating the presence of a flow feature, which is not seen in the simulation. This point coincides with the forward extent of the separation region in the simulation. Peak heating on the aft face of the wedge is in the same location as in the experiment, but the level of heating is underpredicted by approximately a factor of two.

Figure 7 compares the flowfield predicted by the simulation with what is seen experimentally via Schlieren imaging in nitrogen. The simulated flowfield predicts a separation region covering approximately half of the front face of the wedge with multiple vortical structures in the separated flow. The separation shock in the simulated flowfield is a prominent feature, and is not seen in the experiment. The shocks formed in the simulation from the vortical structures travel downstream and impinge on the aft face of the double

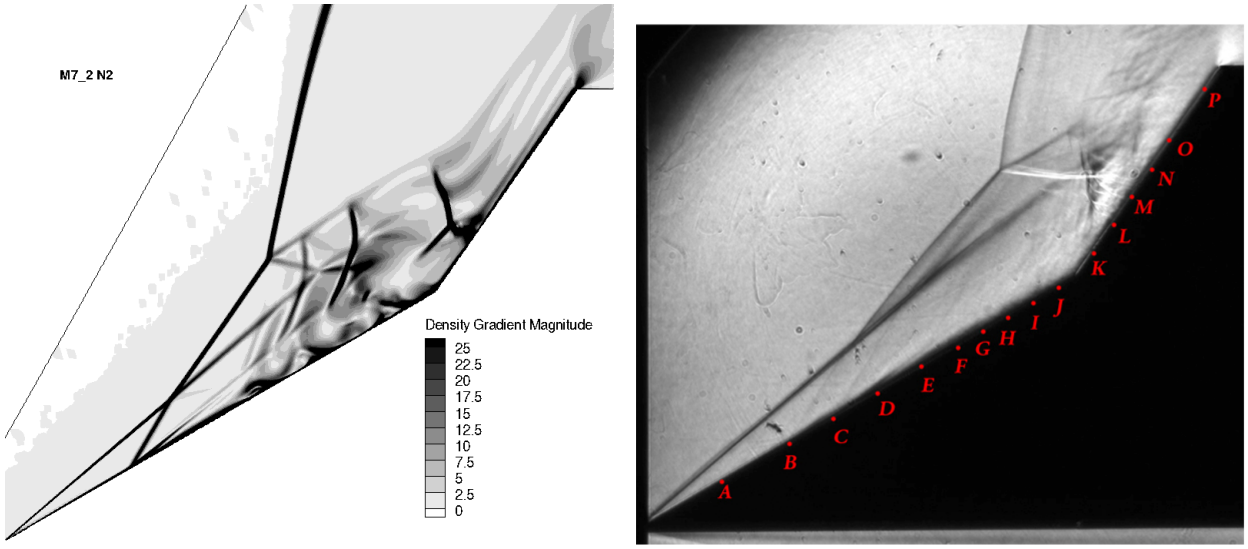

(a) Simulated density gradient magnitude (b) Schlieren from Swantek & Austin,[1] used with permission

Figure 4. Shock visualization of M7_2 free-stream condition in nitrogen at 270 μ**sec**

wedge. Additionally, these traveling shocks displace the bow shock to a larger stand-off distance than was seen experimentally.

Figure 8 compares predicted and experimentally imaged flowfields in air for the M7_8 condition. Here the predicted separation region is much smaller than in the case with nitrogen as the test gas; this is consistent with what is observed in the experiments. Agreement with experiment is good for separation length and separation shock location. The shape and location of the bow shock predicted in the simulation agrees well with that measured in the experiment. However, there are subtle differences at the structure of the triple point. More specifically, the separation shock on the simulation intersects the attached oblique shock earlier. In contrast, the Schlieren image shows that the oblique shocks intersects the bow shock directly, and the separation shock is found entirely behind the oblique shock wave.

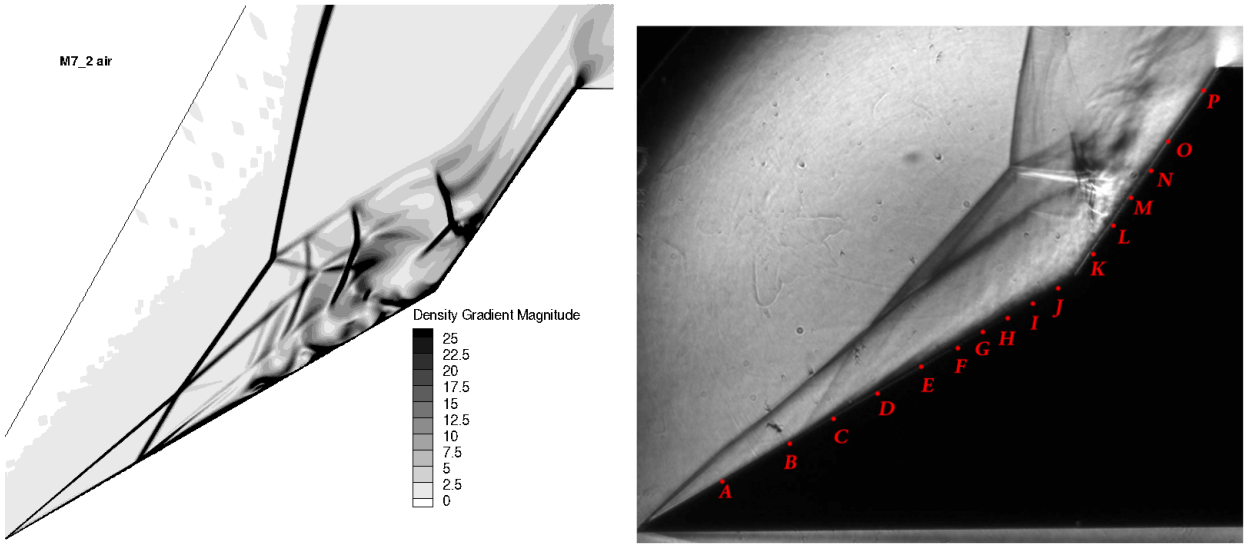

(a) Simulated density gradient magnitude (b) Schlieren from Swantek & Austin,[1] used with permission

Figure 5. Shock visualization of M7_2 free-stream condition in air at 270 μsec

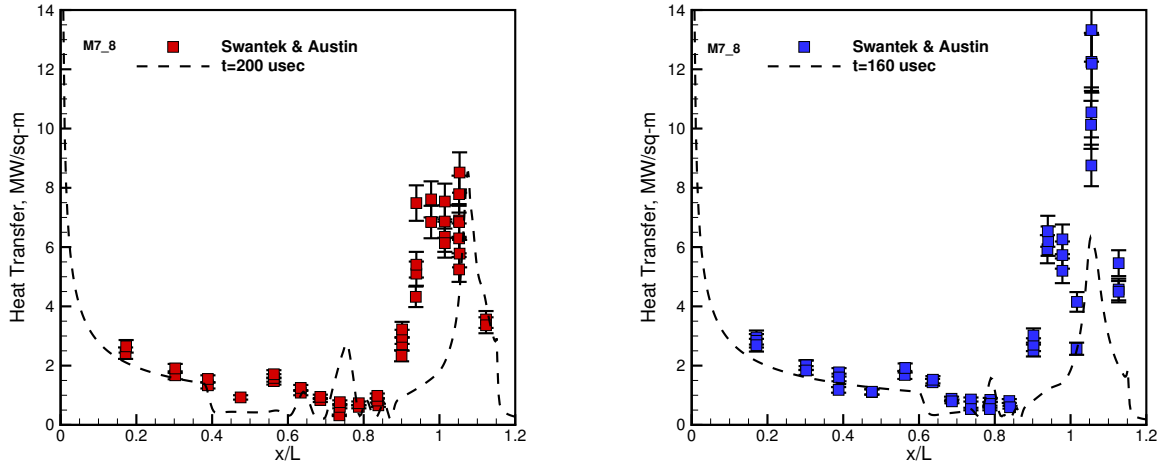

(a) Nitrogen (b) Air

Figure 6. Comparison of instantaneous predicted wall heating with measured values for the M7_8 free-stream condition. Simulation with nitrogen at 200 μsec (a) and air 160 μsec (b) are shown.

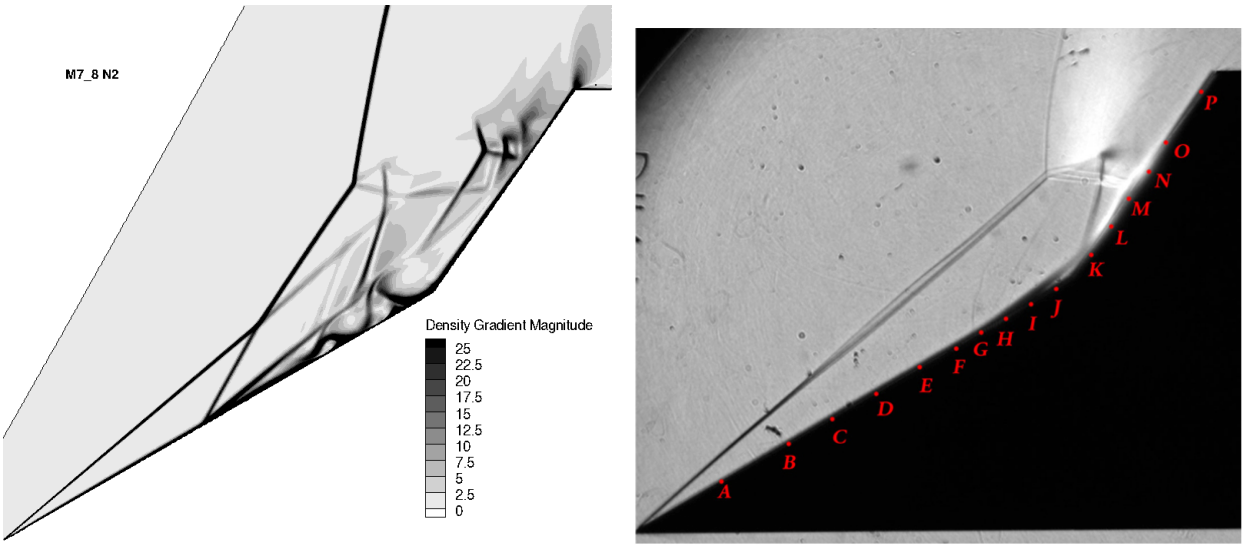

(a) Simulated density gradient magnitude (b) Schlieren from Swantek & Austin,[1] used with permission

Figure 7. Shock visualization of M7_8 free-stream condition in nitrogen at 200 μ**sec**

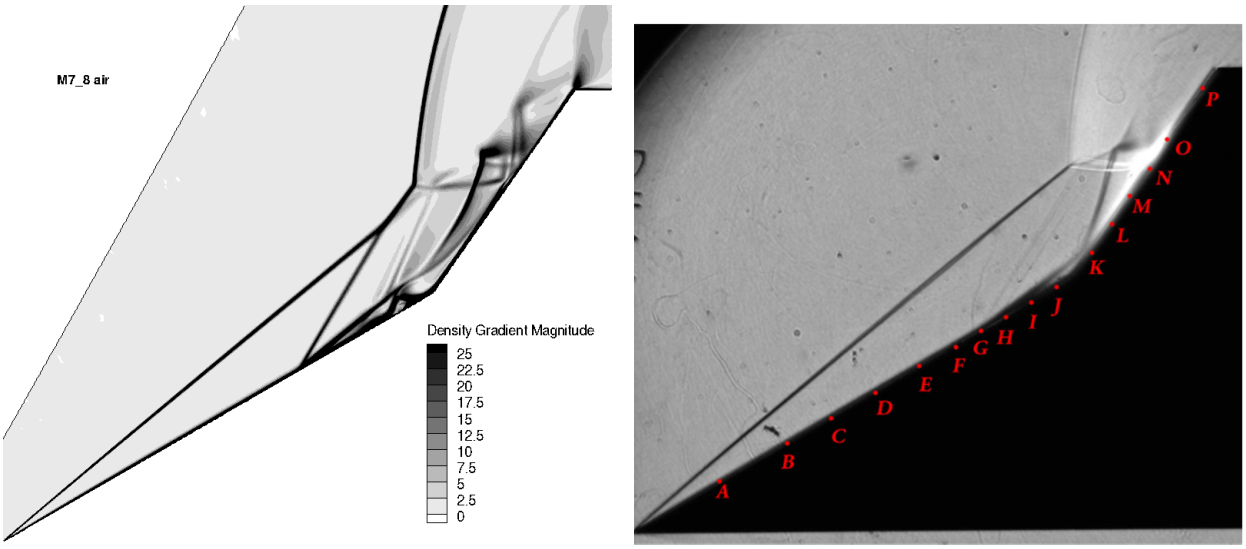

(a) Simulated density gradient magnitude (b) Schlieren from Swantek & Austin,[1] used with permission

Figure 8. Shock visualization of M7_8 free-stream condition in air at 160 μ**sec**

IV. Steady-state Solutions

Experimental test times for the the M7_2 and M7_8 free-stream conditions were 327 μsec and 242 μsec respectively.[1] A characteristic flowtime can be estimated based on the calculated post-shock gas velocity and wedge face length (L=50.8 mm). Based on this characteristic flowtime, the two experiments lasted approximately 12 flowtimes for the M7_2 free-stream condition, and 18 flowtimes for the M7_8 free-stream condition. In order to determine if these measurements represent the steady-state heating on the wedge, we ran our calculations for many flowtimes and compared them to the experimental result. All two-dimensional cases were run to approximately 600 flowtimes to allow the flow to either reach a steady state condition or to obtain an unsteady solution. The results of these numerical experiments are presented in this section.

IV.A. Mach 7, 2 MJ/kg Enthalpy

For the M7_2 free-stream condition, the test gas is modeled as a perfect gas, not allowing any dissociation or energy storage in vibrational energy. Simulations at this free-stream condition reached a periodic steady state solution after approximately 100 flowtimes.

IV.A.1. Simulations in nitrogen

Figure 9 shows the predicted wall heating compared to experimental measurement after a large number of flowtimes have been simulated. The calculation using baseline numerics (second-order accurate inviscid fluxes and a second-order accurate time integration method) significantly underpredicts both the location and amplitude of peak heating. Additionally, the calculation predicts a significantly larger separation zone than the experiments shows.

To investigate the nature of this discrepancy, we examined the effects of numerical dissipation, grid refinement, and temporal discretization. Figure 10 shows the result of adding numerical dissipation to the simulation by reducing the order of accuracy of the inviscid flux scheme. Inadequate numerics can lead to erroneous results when simulating flows that have large gradients over small length scales that are not properly resolved. One must be cautious when interpreting the results of lower order calculations, as any agreement they exhibit may be spurious. In the case of separated hypersonic flows, it has been observed that added dissipation smears gradients in the flow and tends to reduce the extent of separation.[19] In the present simulations, the first-order solution shows better agreement for heating in the separated region, however it overpredicts heating in the attached flow region upstream of the separation point. Additionally, the first-order simulation correctly predicts the level of peak heating but not its location. We believe that any agreement with the measured data is spurious in this case.

Comparing the flowfield predicted by the first-order calculation (Figure 11) with the one predicted by the second-order calculation (Figure 12) sheds some insight into this discrepancy. In both cases the shock which is generated by the separation zone significantly perturbs the bow shock downstream. When compared to the experimental data, the oblique shock location for the second-order calculation is too far upstream. While the first-order calculation places the normal-shock in approximately the correct location, note that all of the fine structures inside the shock layers have been destroyed by the lower-order numerics.

Figure 13(a) shows the predicted heating at two separate instances using a CFL number of 1,000 and 500. As the timestep is refined, the solution does not show a significant change in terms of wall heating. The heating profile is different at the two separate instances but the effect of timestep size is negligible. Figure 13(b) shows the effect of grid-refinement on the steady-state solution. Solutions are plotted on the fine grid at 3 different instances. Like the baseline solution, the refined grid solution is periodic in time with the same wall-heating features present in the separated region as in the baseline solution.

In figure 14, we quantify the periodicity of the numerical prediction on the fine grid. Figure 14(a) shows wall-heating over a span of approximately 4 μsec rendered as a surface over streamwise distance and time. The oscillatory nature of the flowfield is evident in the plot. Furthermore, there are distinct peaks of equal heating level that appear over time. This is more clearly seen when time-traces at fixed locations are plotted as a function of time as in figure 14(b). In this plot, the predicted heat-flux to the wall at the locations of thermocouples A, H, L and M is plotted as a function of time. In this simulation, it appears that the solution obtained using the second-order flux scheme reaches a periodic state with a period of approximately 1.187 msec. Figure 14(c) shows an envelope of heating prediction by plotting the maximum and minimum heating as a function of streamwise distance based on the periodic solution.

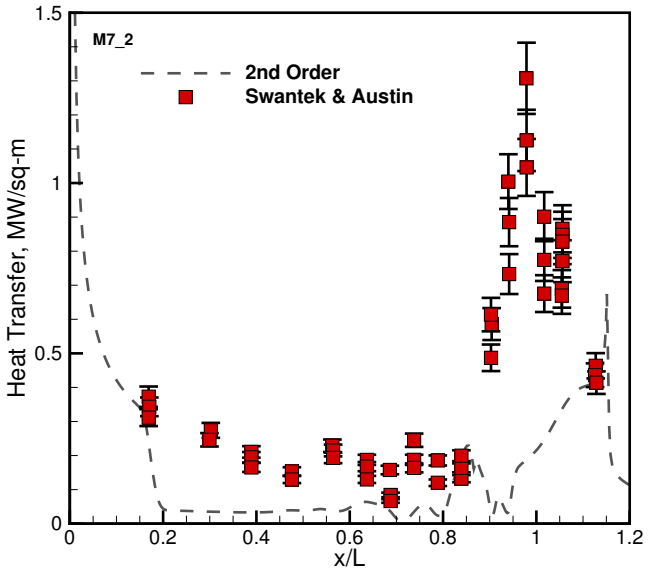

Figure 9. Comparison of second-order accurate simulated and measured wall heating for the M7_2 free-stream condition in nitrogen at 500 flowtimes

The next possibility to investigate is that the long time flowfield may depend on physics that existed in the three-dimensional experiment that are neglected when simplifying the problem to two dimensions. To examine this possibility, a three-dimensional calculation was performed using the modified second-order Steger-Warming flux scheme. It should be noted that while the three-dimensional simulation was run to approximately 50 flowtimes, well beyond the 12 flowtimes of the experiment, it had not yet reached either steady-state or a periodic solution.

Figure 15(a) plots the density gradient magnitude in the domain. Three-dimensional effects are apparent when examining the density gradient contours in the separation region. Additionally, figure 15(b) shows the isosurface defined by spanwise velocity magnitude being equal to the magnitude of the in-plane velocity. This isosurface is then colored by mach number. It is evident by examining this isosurface that there is a region near the surface of the wedge where there the spanwise velocity dominates the flow structure.

Figure 15(c) depicts streamlines on the surface of the wedge. The streamlines near the edge of the wedge all tend to terminate on the edge. Streamlines that originate in the recirculation region coalesce and orient themselves towards the edge of the wedge. This shows that there are persistent three-dimensional effects inside the separated flow region well past the edges.

Figure 15(d) shows the difference between modeling this flowfield as two-dimensional or three-dimensional in terms of wall heat-flux. The three-dimensional simulation predicts a separation region that is smaller than predicted by the two-dimensional simulation. However, it is still larger than the one seen in the experiment. Additionally, the three-dimensional simulation misrepresents peak heating amplitude and location.

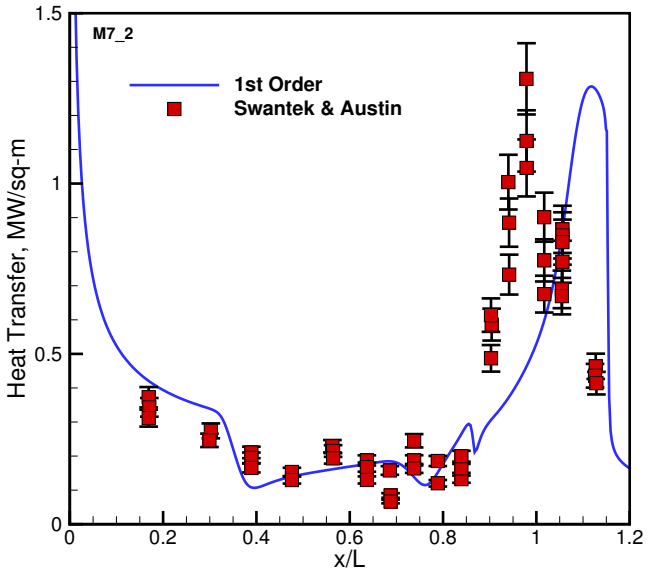

Figure 10. Comparison of measured wall heating and the simulation result obtained at 500 flowtimes with a first-order accurate scheme for the M7_2 free-stream condition in nitrogen.

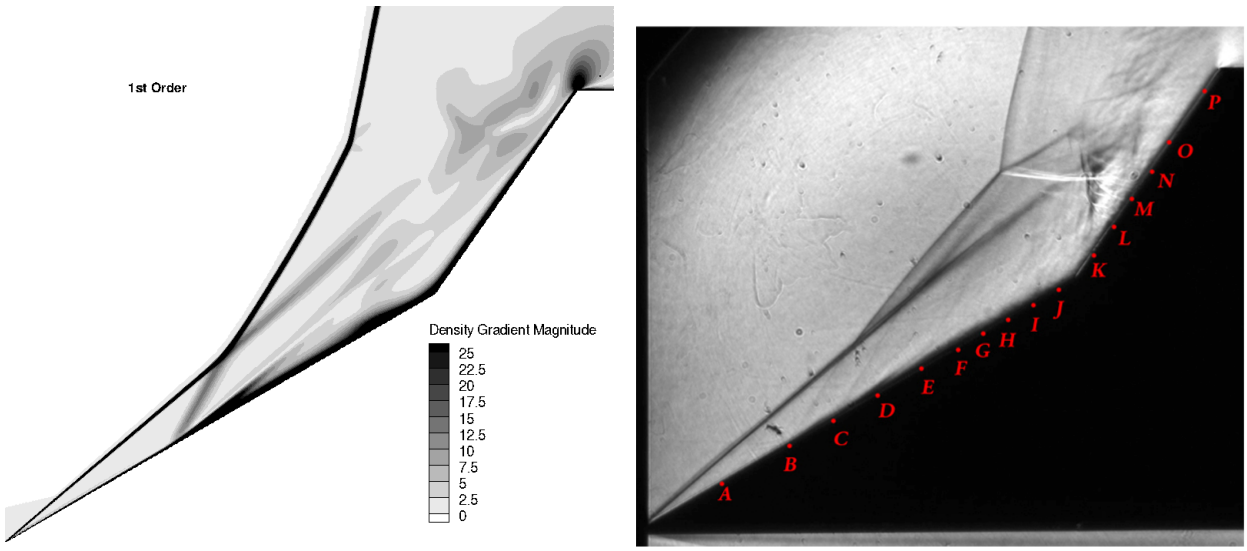

(a) Simulated density gradient magnitude at 500 flowtimes (b) Schlieren from Swantek & Austin,[1] used with permission

Figure 11. Shock-wave visualization for the M7_2 condition in nitrogen using a first-order flux scheme and compared to the experimental Schlieren image.

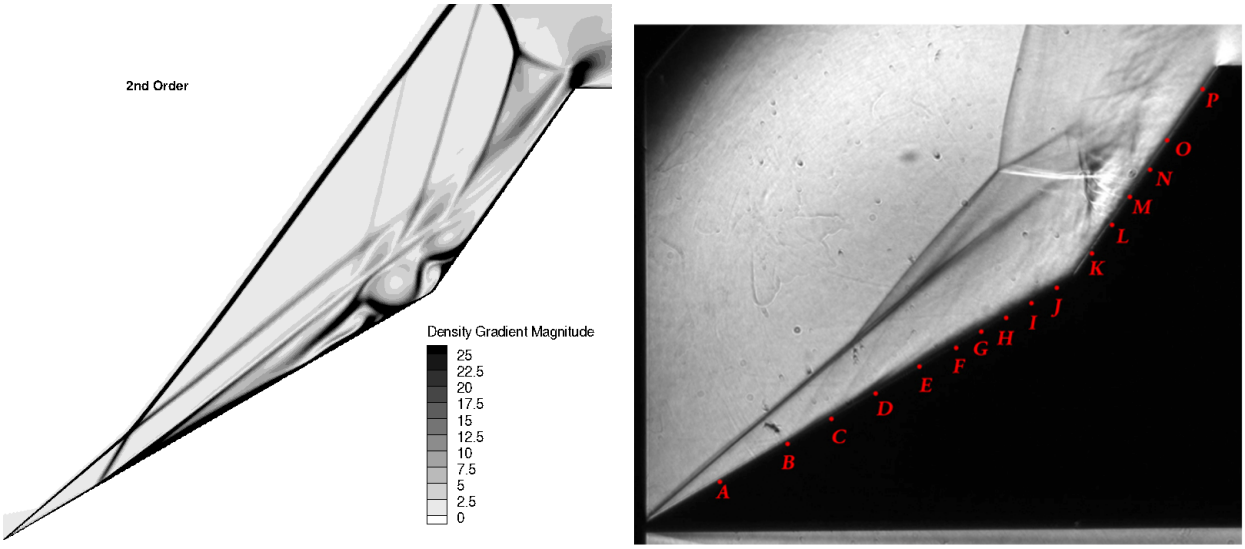

(a) Simulated density gradient magnitude at 500 flowtimes (b) Schlieren from Swantek & Austin,[1] used with permission

Figure 12. Shock-wave visualization for the M7_2 condition in nitrogen using a second-order flux scheme and compared to the experimental Schlieren image.

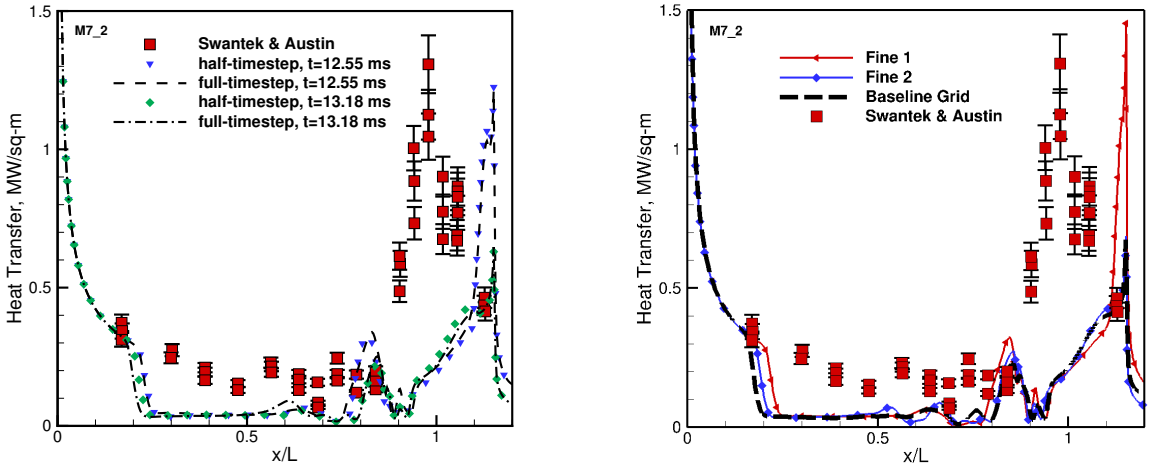

(a) Temporal refinement (b) Grid refinement

Figure 13. Examination of grid and time dependence for the M7_2 condition in nitrogen.

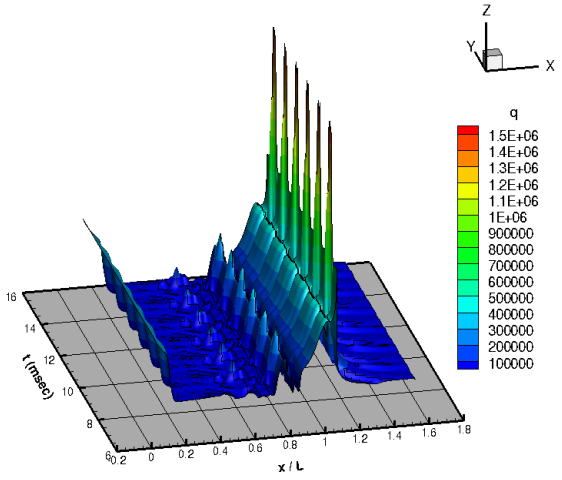

(a) Unsteady heating on the model

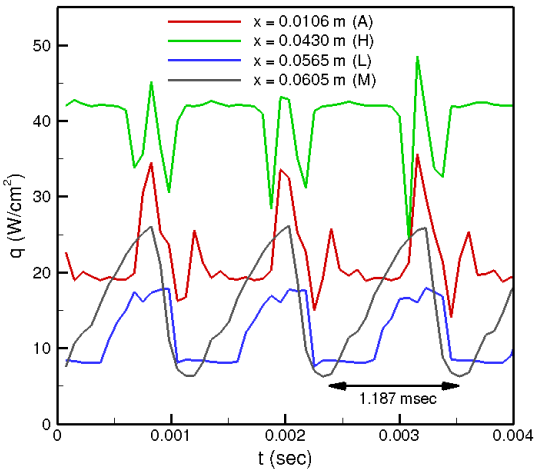

(b) Unsteady heat-flux at select thermocouple locations

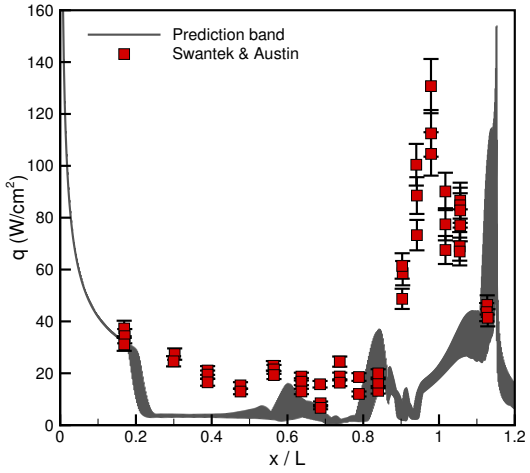

(c) Unsteady heating envelope over streamwise distance

Figure 14. Large time solution periodicity for the M7_2 condition in nitrogen computed on a fine grid

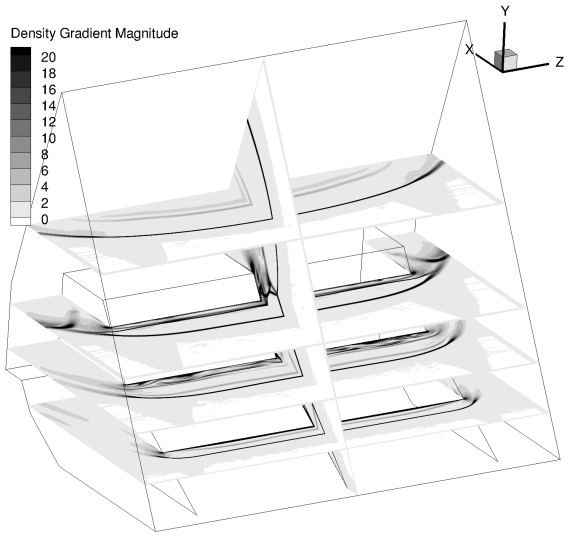

(a) Density gradient magnitude

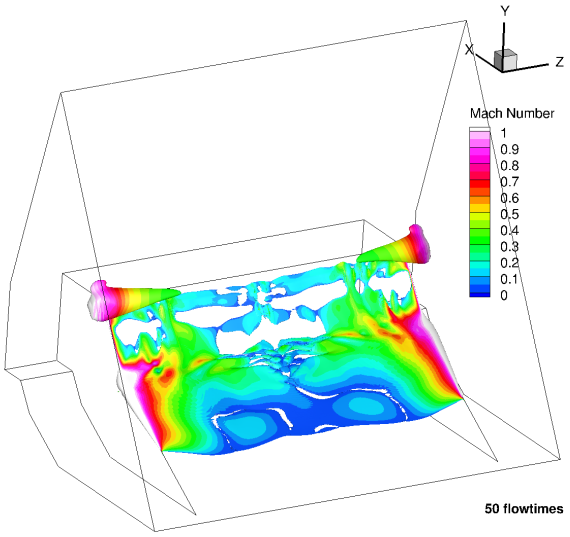

(b) Spanwise velocity ratio, $|w|/\sqrt{u^2+v^2} = 1$, colored by Mach number

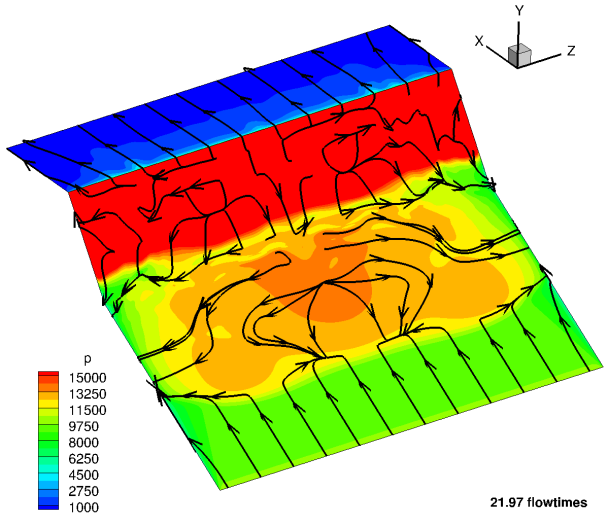

(c) Surface streamlines overplotted with contours of pressure (Pa)

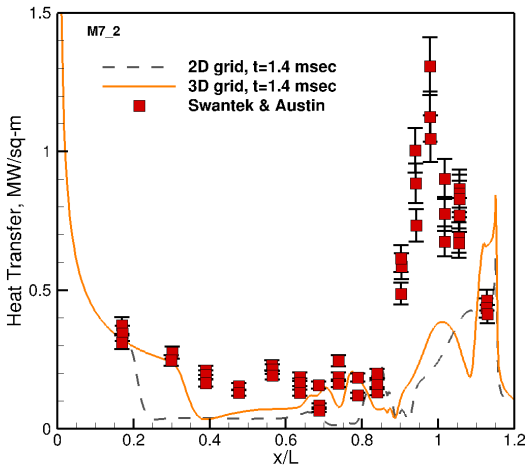

(d) Centerline surface heating

Figure 15. Three-dimensional results of the M7_2 free-stream condition in nitrogen.

IV.A.2. Simulations in air

Changing the test gas to air, the solution still exhibits periodic behavior after many flowtimes. Figure 16 shows the predicted heat flux for air at the M7_2 free-stream condition. Perfect gas calculations are compared to calculations allowing vibrational excitation to determine the validity of the perfect gas assumption at this free-stream condition.

The solutions are nearly identical for surface heating over the forward wedge, which has lower temperatures due to the attached oblique shock. The surface heating downstream of the bow-shock shows poorer agreement, which may be due to the effects of inadequate physical modeling, or may be due to the unsteadiness of the simulation. Both solutions predict a significantly larger separation zone than was seen in the experiment, along with significantly lower heating on the model than was measured in the experiment. Both solutions predict peak heating locations further downstream on the wedge than was measured experimentally.

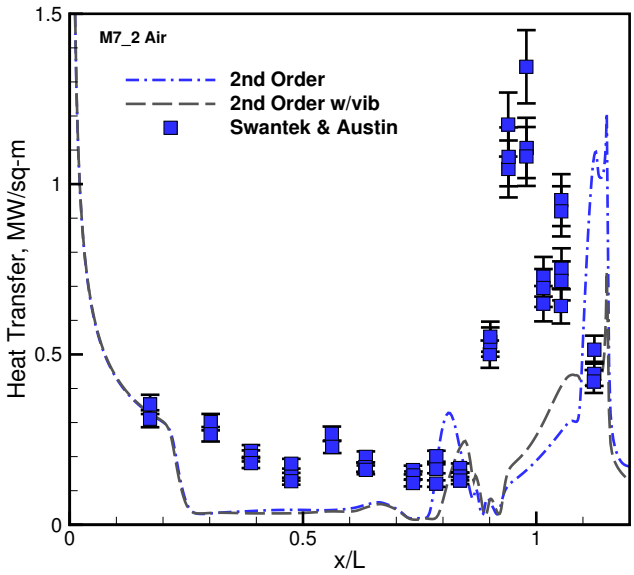

Figure 16. Comparison of simulated heating at 500 flowtimes and measured data for the M7_2 free-stream condition in air.

IV.B. Mach 7, 8 MJ/kg Enthalpy

For the M7_8 free-stream condition, the test gas is modeled as a "real" gas, including effects of vibrational excitation, dissociation and recombination. Simulations at this free-stream condition reached a steady state solution after approximately 300 flowtimes.

IV.B.1. Simulations in nitrogen

Many of the results from the lower enthalpy calculations at a large number of flowtimes carry over to the high enthalpy free-stream condition. As Figure 17 shows, the second-order calculation greatly underpredicts the peak heating amplitude and overpredicts the extent of the separation region. Adding dissipation by lowering the order of accuracy of the numerical method results in a higher levels of heating on the forward face of the wedge upstream of the separation region. Separation is predicted to occur much further downstream on the forward wedge as a result of added dissipation. Additionally, the added dissipation from the lower order scheme results in predictions of peak heating amplitude that are closer to what was seen in experiment.

Flowfields at this free-stream condition (Figures 18 and 19) show similar character to the flowfields at the lower enthalpy free-stream condition, albeit with smaller shock angles. Here again, the separation shock predicted by the higher-order numerics interacts with the bow-shock more downstream than is predicted by

the first-order calculation, or was observed in experiment. The first-order calculation loses nearly all of the detail of the small scale structures in behind the shock and inside the separation zone.

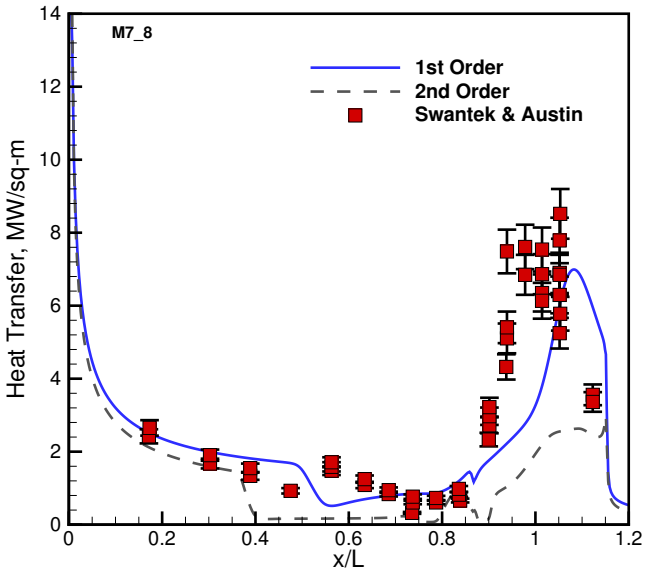

Figure 17. Comparison of simulated heating at 870 flowtimes and measured data for the M7_8 free-stream condition in nitrogen.

IV.B.2. Simulations in air

Of all the conditions examined, the M7_8 free-stream condition in air shows the largest discrepancy between the predicted wall heating and the measured wall heating. Note that this is the highest free-stream enthalpy condition. Figure 20 shows that simulations miss the peak heating level, even though they do predict peak heating location. Consistent with results at other conditions, the second-order calculation predicts a larger separation zone and lower peak heating than the experimental measurements show, and also shows lower heating levels on the forward face of the double wedge.

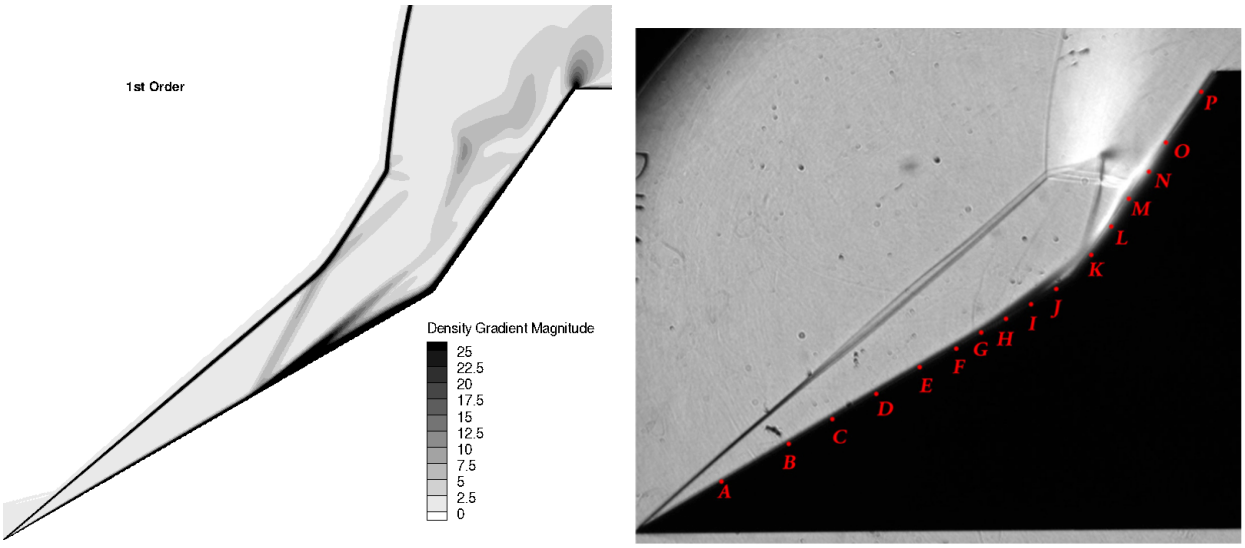

(a) Simulated density gradient magnitude at 870 flowtimes (b) Schlieren from Swantek & Austin,[1] used with permission

Figure 18. Shock-wave visualization, M7_8 first-order in nitrogen

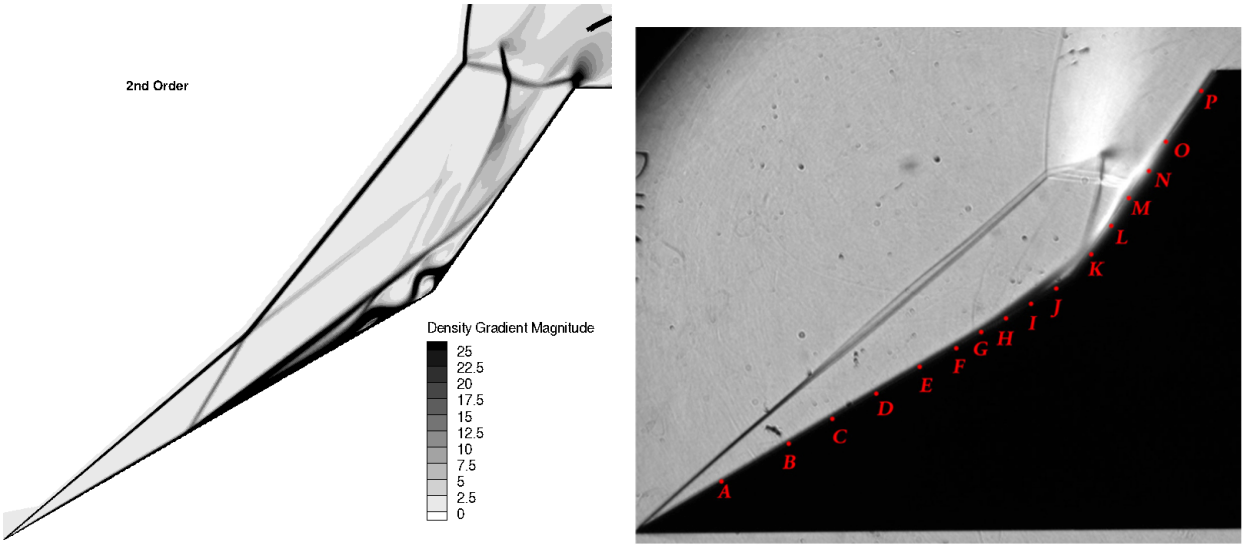

(a) Simulated density gradient magnitude at 870 flowtimes (b) Schlieren from Swantek & Austin,[1] used with permission

Figure 19. Shock-wave visualization, M7_8 second-order in nitrogen

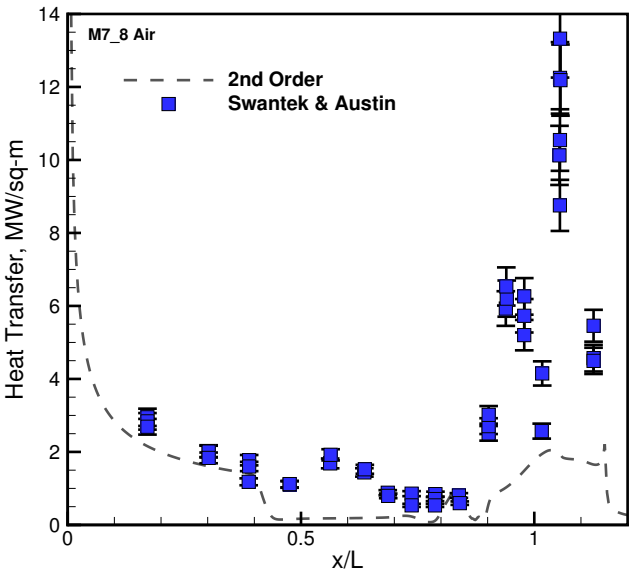

Figure 20. Comparison of simulated heating at 870 flowtimes and measured data for the M7_8 free-stream condition in air.

V. Conclusions

Predicted wall heating for the M7_2 and M7_8 free-stream conditions in both air and nitrogen showed reasonable agreement with experimental heating measurements when the simulations were terminated approximately at the same time as when the experiment ended, however there were notable differences in predicted and measured flowfield structure. Continuing these simulations to steady-state resulted in predictions of wall heating and flowfield structure that were inconsistent with the experimental results. The M7_2 simulations converged to a periodic solution while M7_8 simulations converged to a stationary flowfield. Grid refinement and timestep refinement studies did not indicate deficiencies due to grid construction or temporal integration scheme. Increasing numerical dissipation resulted in better qualitative agreement with experiment, however this result is spurious since the solution no longer retains any of the small-scale physical structures important to these double wedge flows. It is clear from this examination that these flowfields are very sensitive to numerical dissipation or numerical error, and that great care must be taken when selecting flux schemes and constructing grids.

Three-dimensional simulations of the complete test article at the M7_2 free-stream condition in nitrogen showed appreciable spanwise velocities in the separation region. It would appear that the ends of the model provide pressure relief, allowing the separation zone to thin by allowing mass to flow around the sides of the test article. In addition to thinning the separation region, this spanwise velocity at the wall also induced streamwise vorticity in the boundary layer. Further attempts to replicate the experimental results should be time-accurate, three dimensional, and averaged over an appropriate sampling interval to provide a more direct comparison the experimental results.

References

[1]Swantek, A. and Austin, J., "Heat Transfer on a Double Wedge Geometry in Hypervelocity Air and Nitrogen Flows," *Proceedings of the 50th Annual Aerospace Sciences Meeting*, January 2012.

[2]Badr, M. A. and Knight, D. D., "Shock Wave Laminar Boundary Layer Interaction Over a Double Wedge in a High Mach Number Flow," *Proceedings of the 52nd Aerospace Sciences Meeting*, January 2014.

[3]Patil, V. N., Levin, D. A., Gimelshein, S. F., and Austin, J. M., "Study of shock-shock interactions for the HET facility double wedge configuration using the DSMC approach," *43rd Fluid Dynamics Conference*, June 2013.

[4]Nompelis, I., Drayna, T., and Candler, G., "A Parallel Unstructured Implicit Solver for Hypersonic Reacting Flow Simulation," *17th AIAA Computational Fluid Dynamics Conference*, 2014/05/28 2005.

[5]Olejniczak, J., Candler, G. V., Wright, M. J., Leyva, I., and Hornung, H. G., "Experimental and Computational Study of High Enthalpy Double-Wedge Flows," *Journal of Thermophysics and Heat Transfer*, Vol. 13, No. 4, 1999, pp. 431–440.

[6]Olejniczak, J., Candler, G. V., Wright, M. J., Hornung, H. G., and Leyva, I., "High Enthalph Double-Wedge Experiments," *Proceeding of the AIAA Advanced Measurement and Ground Testing Technology Conference*, New Orleans, LA, 1996.

[7]Nompelis, I., Candler, G. V., Holden, M. S., and Wadhams, T. P., "Computational Investigation of Hypersonic Viscous/Inviscid Interactions in High Enthalpy Flows," *Proceedings of the 36th AIAA Thermophysics Conference*, 2003.

[8]Coblish, J. J., Smith, M. S., Hand, T., Candler, G. V., and Nompelis, I., "Double-Cone Experiment and Numerical Analysis at AEDC Hypervelocity Wind Tunnel No. 9," *AIAA Paper No. 2005-0902*, January 2005.

[9]Vincenti, W. G. and Kruger, C. H., *Introduction to Physical Gas Dynamics*, Krieger Publishing Company, 1965.

[10]Millikan, R. C. and White, D. R., "Systematics of Vibrational Relaxation," *Journal of Chemical Physics*, Vol. 39, 1963, pp. 3209–3213.

[11]Park, C., *Nonequilibrium Hypersonic Aerothermodynamics*, John Wiley, 1990.

[12]Blottner, F., Johnson, M., and Ellis, M., "Chemically Reacting Viscous Flow Program for Multi-Component Gas Mixtures," Tech. Rep. SC-RR-70-754, Sandia Laboratories, 1971.

[13]MacCormack, R. W. and Candler, G. V., "The Solution of the Naviers-Stokes Equations Using Gauss-Seidel Line Relaxation," *Computers and Fluids*, Vol. 17, No. 1, 1989, pp. 135–150.

[14]Subbareddy, P. K. and Candler, G. V., "A fully discrete, kinetic energy consistent finite-volume scheme for compressible flows," *Journal of Computational Physics*, Vol. 228, No. 5, 2009, pp. 1347 – 1364.

[15]Wright, M. J., Candler, G. V., and Bose, D., "Data-Parallel Line-Relaxation Method for the Navier-Stokes Equations," *AIAA Journal*, Vol. 36, No. 9, September 1998, pp. 1603–1609.

[16]Swantek, A., *The role of aerothermochemistry in double cone and double wedge flows*, Ph.D. thesis, University of Illinois at Urbana-Champaign, 2012.

[17]Dufrene, A., Sharma, M., and Austin, J. M., "Design and Characterization of a Hypervelocity Expansion Tube Facility," *Journal of Propulsion and Power*, Vol. 23, No. 6, 2014/05/24 2007, pp. 1185–1193.

[18]Nompelis, I., Candler, G., Holden, M., and Wadhams, T., "Numerical Simulation of High-Enthalpy Experiments in the LENS X Expansion Tube Facility," *42nd AIAA Aerospace Sciences Meeting and Exhibit*, January 2004.

[19]Druguet, M.-C., Candler, G., and Nompelis, I., "Comparison of Physical Models in Computations of High-Enthalpy Double-Cone Flows," *9th AIAA/ASME Joint Thermophysics and Heat Transfer Conference*, June 2006.